ELSEVIER

Journal of Nuclear Materials 246 (1997) 171–179

journal of nuclear materials

The behaviour of helium in neutron irradiated beryllium: a molecular dynamics study

J.-M. Cayphas [a], M. Hou [a,*], L. Coheur [b]

[a] *Physique des Solides Irradiés CP234, Université Libre de Bruxelles, Bd du Triomphe, B-1050 Brussels, Belgium*
[b] *LHMA, CEN / SCK, Boerentang 200, B-2400 Mol, Belgium*

Received 30 January 1997; accepted 25 April 1997

Abstract

An atomic scale study is presented of the trapping of helium atoms by vacancies and di-vacancies in beryllium. Constraint molecular dynamic methods are used to estimate formation energies, helium-vacancy binding energies, migration energies as well as for direct evaluation of Helmholtz free energy differences. The beryllium cohesion is described with a model derived from the second moment tight binding approximation, while the helium–beryllium interaction is based on the embedded atom model and a mean field approximation. It is found that up to ten helium atoms may be bound to one single vacancy and up to fourteen to a di-vacancy. The possible trapped helium configurations are identified. The thermodynamic stability of such helium-vacancy clusters is found to be only little dependent on the vibrational entropy in a temperature range from 0 K to 1270 K, which shows that 0 K energetic calculations already provide reasonable free energy estimates. This suggests that the method can be used to study helium retention in large systems with extended defects at temperatures relevant to fission and fusion technologies. © 1997 Elsevier Science B.V.

1. Introduction

Beryllium is widely used as moderator and reflector of nuclear fission research reactors generally at temperatures between 50 and 150°C. Its use is also seriously considered in the future magnetic fusion reactor as plasma facing material on diverter and first wall and as neutron multiplier in the blanket. For all these uses, a thorough knowledge of the behaviour of beryllium under neutron irradiation is of primary importance. The most damaging effect on the properties of the beryllium when it is subjected to a neutron flux is coming from the production of helium inside the material as the result of the two nuclear reactions: (n, 2n) and (n, α) [1].

A relatively large amount of experimental data is available from low temperature irradiation experiments. The observed dimensional changes are limited and increase linearly with the high energy neutron fluence. The scattering between these data is small. If the swelling is probably not a cause of concern at low temperature, the ductility of the material which is already very small before irradiation is practically reduced to zero after a rather low neutron fluence. This effect seems also to be essentially due to the presence of increasing concentrations of helium in the material. Data from irradiation experiments at the elevated temperatures of interest for the fusion reactor (350–700°C) are scarce and their scattering much larger. Annealing samples previously irradiated at low temperature has been tried in order to increase the swelling data at elevated temperature. The scattering in the data is not reduced. However, phenomenological relationships were derived [2–5]. Some of them were critically reviewed by Nardi [6]. Recently, a computer code (ANFIBE) based on an existing code for the modelling of gas behaviour in fuel elements has been proposed [7]. It has been observed that the properties including the swelling behaviour are very sensitive to the structural (grain size, oxide particle distribution) and fabrication (purity, oxide content) parameters [8]. The differences between the materials tested by the various investigators can probably explain the scatter of the data.

* Corresponding author.

PII S0022-3115(97)00102-5

Presently, new irradiation experiments are being carried out on different kinds of beryllium samples to get a more precise insight into the phenomena occurring during irradiation at elevated temperature [9,10]. Complementary to these experiments, the present work is part of a project undertaken to understand basic first steps in the process of the progressive helium concentration increase during neutron irradiation and to evaluate the influence of the temperature on them. One of these steps, on which the present paper focuses is the possible precipitation of helium at point defects. This is analysed in detail by means of atomic scale modelling.

In Section 2, the methods and the models used are described which allow a pertinent description of the helium-vacancy interaction in beryllium. Energetic calculations are discussed in Section 3 both ignoring and taking vibrational entropy effects into account.

Conclusive comments are provided in Section 4.

2. The methods

2.1. Molecular dynamics

A convenient way to handle an atomic system which evolution at the atomic scale is governed by temperature induced fluctuations is to consider the electronic system as a reservoir embedding the ionic system. The solid may then be described by means of a canonical ensemble where the ionic system exchanges energy with a heat bath formed by the electrons. Such a situation is described by the so-called extended system method [11,12] in which one degree of freedom is introduced, acting on the external system (the electrons in the present situation) of the physical system of N particles (the ions). The corresponding hamiltonian from which the equations of motion are derived may be written as

$$H = \sum_i \frac{p_i^2}{2m_i s} + V(r) + \frac{p_s^2}{2Q} + gkT \ln s, \tag{1}$$

where s is the additional degree of freedom, p_s its conjugate momentum, Q an inertial factor, and $V(r)$ a potential term. The other potential term, $gkT \ln s$ has a functional dependence on s such that the partition function derived from Eq. (1) is that of the canonical NVT ensemble. It should be noted that Eq. (1) reduces to the hamiltonian of the NVE ensemble from which the Newton equations of motion are derived when fixing $s = 1$.

In the present work, the equations of motion are integrated numerically according to the fifth order Nordsieck predictor–corrector algorithm [13]. The simulation boxes used typically contain one thousand atoms. Neighbour lists are prepared for the force calculations and periodically refreshed according to the Verlet algorithm [14]. It may be noted that its combination with a linked-cell algorithm [15] is only efficient for larger systems than used in the present work. The square root of the potential and force functions are tabulated. In such a way, forces may be estimated by linear interpolation with comparable accuracy over the whole range of interaction. Born–von Karman periodic boundary conditions are applied [16] in order to simulate an infinite system.

2.2. The potentials

The major parameter which governs the dynamics of the atomic interactions is the potential from which the interatomic forces derive. In the case of beryllium, the particles interact via an N-body potential, the attractive part of which is taken identical to that used in a cohesion model derived from the second moment approximation of the tight binding scheme [17]. This scheme was adapted to hcp metals [18] and the potential energy may be written as

$$E_{\text{tot}} = \tfrac{1}{2} \sum_{ij} V(R_{ij}) - \sum_i f(\rho_i), \tag{2}$$

where the summations run over all N atoms. $V(R_{ij})$ represents the pair interaction between atoms i and j separated by a distance R_{ij} and f is an attractive many body function. In the tight binding scheme, f is interpreted as a sum of squares of hopping integrals and ρ_i is written as a sum of pair potentials

$$\rho_i = \sum_j \Phi(R_{ij}). \tag{3}$$

In the second moment approximation, f is proportional to the square root of ρ. It is shown in [18], however, that this implies the elastic constant C_{12} to be larger than C_{66} which is not the case of hcp beryllium. Therefore, the following functional dependence of f on ρ is preferred

$$f(\rho) = \sqrt{\rho}\,(1 + A\rho), \tag{4}$$

where A is a suitably chosen constant. Following [19], $V(r)$ and $\Phi(r)$ are written as cubic splines

$$V(r) = \sum_{k=1}^{n} A_k (R_{ak} - r)^3 H(R_{ak} - r), \tag{5a}$$

$$\Phi(r) = \sum_{k=1}^{m} B_k (R_{bk} - r)^3 H(R_{bk} - r), \tag{5b}$$

where R_{ak} and R_{bk} are the knot points, $n = 7$ and $m = 5$. Eqs. (5a) and (5b) thus have 24 adjustable parameters which allow a fitting of the potential on macroscopic and microscopic properties of the material. The values of these parameters and of the parameter A (Eq. (4)) are tabulated for beryllium and other hcp metals in [19].

The embedded atom model (EAM) is used in the framework of the effective medium theory to model helium in a beryllium matrix [20–25]. In the effective medium theory, it is considered that the energy of an atom embed-

ded in a system of interacting atoms depends on the electron density of the atoms surrounding atom i. According to Ref. [22], one writes

$$E_i = E(\bar{n}_i), \tag{6}$$

where $\bar{n}_i$ is the average of the density contributions Δn_j from the neighbouring atoms in the region occupied by atom i,

$$\bar{n}_i = \sum_{j \neq i} \langle \Delta n_j \rangle_i \tag{7}$$

In the low electron density limit, the embedding energy function increases linearly with the background electron density $n(r)$ [26],

$$V(r) = \alpha n(r). \tag{8}$$

If, as suggested in Ref. [27], the electron density at position r is written as

$$\bar{n}(r) = n_0 e^{-\eta(r-r_0)}, \tag{9}$$

where n_0 is the electronic density minimising the energy of the system, η a constant and r_0 the Wigner–Seitz cell radius, the embedding energy takes the form of a Born–Mayer potential

$$V(r) = Ae^{-\beta r}. \tag{10}$$

Using, in Eq. (9), the parameter values $\alpha = 200$ eV bohr^3 for embedded helium [24], $r_0 = 2.633$ bohr, $n_0 = 0.0076$ bohr^{-3} and $\eta = 1.928$ bohr^{-1} [27], one deduces the values of the parameters A = 243.5 eV and $\eta = 3.6433$ Å^{-1} in Eq. (10). These values are substantially different from those deduced from a least square fit of TFD data in [28] ($A = 412$ eV and $\eta = 4.03$ Å^{-1}). The latter predicts a too high energy at small separations and becomes similar to the effective medium estimate at distances close to the first neighbour distance in beryllium. Finally, a Born–Mayer model potential is also used for the He–He interaction of which parameters are determined on the basis of a statistical theory using electron densities from Hartree–Fock calculations [29].

2.3. Energetic calculations

The kinetics of point defects and the stability of point defect clusters depend on a limited number of parameters as formation enthalpies, migration enthalpies and Helmholtz free energies, which can be estimated.

Self-interstitial diffusion in beryllium is found experimentally to obey an Arrhenius law fairly well [30,31], consistent with a mono-vacancy mechanism. This is an indication that the vacancy formation and migration enthalpies are only weakly dependent on temperature and they can be reasonably estimated at 0 K. No such indication is available about the formation of point defect clusters for which temperature dependent free energy calculations are thus necessary. Equilibrium configurations 0 K are estimated with the quasi dynamic procedure including damping forces first suggested by Bennet [32]. The method allows for vacancy and interstitial formation energy calculation, which are given by

$$E^F = N_0 \left(\frac{U_D}{N_D} - \frac{U_0}{N_0} \right), \tag{11}$$

where N_0 and N_D are the number of particles in the perfect and the defective solid, respectively, and U_0 and U_D are the 0 K energies per atom in the perfect and the relaxed defective solid, respectively.

Migration energies are a little more difficult to estimate. Indeed, they are defined as the difference between the configuration energies of the system with the migrating species at the potential saddle point and in the initial potential well. The problem is that, except in very simple situations like, say, the vacancy diffusion mechanism in a cubic metal, the saddle point cannot be identified unambiguously on the only basis of geometrical considerations and their location is thus not obvious. In principle, it can be identified by following the real trajectory of the diffusing particle in time, but this can only be done by molecular dynamics when the jump frequency is high enough which, practically, only happens in a limited number of situations.

Therefore, the following procedure is employed. The initial and the final jump positions of the migrating species being known, a rectangular parallelopipedic box is constructed, using these two points as the edges of one diagonal. A number of intermediate equidistant planes is then considered from one edge of the box to another, parallel to one of its face. Their number depends on the desired accuracy. The points inside the box and inside each of these planes where the helium configuration energy is minimum are then determined. This is done by using the damping technique mentioned above for a helium atom constrained to move inside one of these planes, and the procedure is repeated in each of them. The saddle point is located between the two neighbouring planes where the so-determined minimum energies are the highest and its value is evaluated by interpolation. In the situations discussed in the present work, ten to twelve intermediate planes are sufficient in order to evaluate the saddle point energy with an accuracy of 0.15 eV.

Free energy differences are calculated at a given non zero temperature by the constrained molecular dynamic method described in Ref. [33]. In this method, the free energy difference is derived from a direct evaluation of a mean thermodynamic force. It takes advantage from the fact that thermodynamic functions can be partitioned among their projection onto atomic individual sites [34] and the Helmholtz free energy of a system may thus be written as

$$A = \sum_i (U_i + A_i), \tag{12}$$

where the summation runs over all sites. U_i is the potential energy at site i and A_i is the vibrational contribution to

the free energy at site i. The expectation of the mean thermodynamic force f_i acting on atom i is defined as the negative gradient of the total free energy with respect to the position of atom i:

$$f_i = -\nabla_i A. \tag{13}$$

Thus, starting from the projection of the canonical partition function Q on site i, the mean thermodynamic force may be written as

$$f_i = -\frac{1}{\beta}\frac{\nabla_i Q}{Q} = -\frac{\int \nabla_i U e^{-\beta U} d\Gamma}{\int e^{-\beta U} d\Gamma} = -\langle \nabla_i U \rangle, \tag{14}$$

where Γ represents the spatial coordinates. The thermodynamic force f_i thus appears to be equal to the negative of the canonical mean of the gradient of the internal energy with respect to the position of atom i. Eq. (14) may be computed by molecular dynamics (as well as by Monte Carlo) and, since canonical and microcanonical averages converge in the thermodynamic limit, Eq. (14) may be evaluated in both ensembles. It thus appears that the reversible work of the mean thermodynamic force to constrain the system from one configuration to another represents the associate free energy difference and it can be obtained along any reversible path between the initial and the final configuration. It thus applies to the migration of an atom from one site to another and may be used to discuss the stability of point defect clusters as a function of temperature.

3. The results

3.1. Formation energies

Formation energies were computed for mono-vacancies, di-vacancies, helium interstitials at different geometrically plausible equilibrium sites, helium clusters decorating one mono-vacancy or one di-vacancy inside their associated Wigner–Seitz cells as well as in neighbouring octahedral sites.

The different possible helium interstitial positions in hcp lattices, as deduced from the lattice symmetry, are shown in Fig. 1. These sites are the octahedral (O), basal octahedral (BO), tetrahedral (T), basal tetrahedral (BT) and the so-called crowdion (C) sites. Fig. 2a–j show the equilibrium positions found for clusters of two to five helium atoms decorating a mono-vacancy and a di-vacancy and confined inside the associated Wigner–Seitz cells. These are the lowest energy configurations found. Owing to the specific hcp stacking, the helium configurations around vacancies and di-vacancies cannot be obviously deduced on the only basis of geometric considerations. From symmetry considerations, however, variants of the configurations displayed, with identical energy, can be deduced which are not shown. There are three variants to Fig. 2a, two variants of Fig. 2b–d, one of Fig. 2e, two of Fig. 2f, two of Fig. 2g, one of Fig. 2h, four of Fig. 2i and of Fig. 2j.

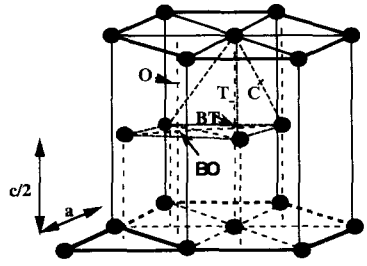

Fig. 1. An hexagonal close packed unit cell. The various stable and unstable equilibrium interstitial locations are shown. O refers to an octahedral site, BO to a basal octahedral site, T to a tetrahedral, BT to a basal tetrahedral and C to a so-called crowdion location.

The formation energies obtained with the model potential described above are given in Table 1. Several features

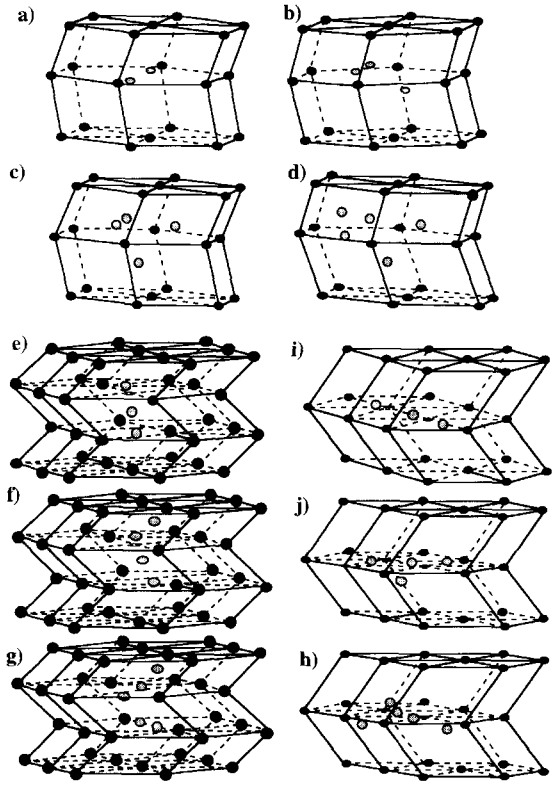

Fig. 2. The various helium-vacancy cluster configurations found stable at 0 K. The black dots represent beryllium atoms, the grey ones represent helium atoms. The vacancies are represented by open squares. Solid and dashed lines are drawn in order to guide the eye. (a–d) helium atoms decorate one mono-vacancy; (e–g) they decorate a di-vacancy of type b; (i–h) they decorate a di-vacncy of type a.

Table 1
Formation energies (noted E^F, given in eV) of point defects and point defect clusters at 0K. He_n–V_m stands for a cluster formed by n helium atoms and m vacancies. V_{2a} stands for a di-vacancy in a basal plane and V_{2b} for a di-vacancy not in a basal plane. The uncertainty of the estimates is one digit on the last decimal

Defect	E^F	Defect	E^F	Defect	E^F	Defect	E^F
V	1.13	He–V	4.8	He–V_{2a}	5.3	He–V_{2b}	5.2
V_{2a}	1.58	He_2–V	10.4	He_2–V_{2a}	9.2	He_2–V_{2b}	9.7
V_{2b}	1.51	He_3–V	15.6	He_3–V_{2a}	14.1	He_3–V_{2b}	14.0
He at O	6.8	He_4–V	21.4	He_4–V_{2a}	19.5	He_4–V_{2b}	20.7
He at BO	unstable	He_5–V	28.0	He_5–V_{2a}	24.8	He_5–V_{2b}	26.8
He at T	unstable	He_6–V	unstable	He_6–V_{2a}	unstable	He_6–V_{2b}	unstable
He at BT	unstable						
He at C	unstable						

clearly come out of this table. First, among the a priori geometrically plausible helium interstitial sites at 0 K, only the octahedral sites are found to be stable, which is consistent with a repulsive pair potential decreasing with distance. Second, two non equivalent types of di-vacancies are possible (noted V_{2a} and V_{2b} in Table 1) of which formation energies are found to be similar although a sizeable difference is noticed.

The binding energy of a defect cluster formed by n helium atoms and m vacancies may be written as

$$E^B(He_n - V_m) = mE^F(V_m) + nE^F(He) - E^F(He_n - V_m). \quad (15a)$$

Similarly, the binding energy of one helium atom to a cluster formed by n helium atoms and m vacancies may be written as

$$E^B_{He}(He_n - V_m) = E^F(He_n - V_m) + E^F(He) - E^F(He_{n+1} - V_m). \quad (15b)$$

Both binding energies are given in Table 2.

Using Eq. (15a), one finds a binding energy for di-vacancies is 0.68 eV if it sits in a basal plane and 0.75 eV otherwise. As helium-vacancy clusters are concerned, the binding energies estimated using Eq. (15b) are not found to be monotonically decreasing with the number of helium atoms in the cluster. This is better illustrated in Fig. 3 which displays the binding energy of a helium atom residing inside the same Wigner–Seitz cell as a function of the number of atoms already decorating a mono-vacancy or a di-vacancy. The general tendency for the binding energy is to tend to zero with increasing number of decorating helium atoms but the fluctuations observed are significantly larger than the uncertainties. Moreover, it cannot be intuitively predicted whether the binding energy will be the highest in a mono-vacancy, a di-vacancy of type a or of type b. A similar non-monotonic dependence was already noticed in cubic metals [35,36]. On the other hand, the repulsive energy between the helium atoms within the same Wigner–Seitz cell increases with their number and on the other hand, it is lowered by the symmetry of their spatial configuration. The effect of this balance on the binding energy cannot be deduced from geometrical considerations.

The results also show that, at 0 K, no more than five helium atoms can be bound to a mono-vacancy or a di-vacancy if they sit inside the associated Wigner–Seitz cell. This does not rule out the possibility for helium in neighbouring octahedral sites to be bound to a vacancy or a di-vacancy, and this problem is now examined in detail.

Taking all configurations found of helium in the Wigner–Seitz cells of a vacancy or of the di-vacancies as displayed in Fig. 2, the binding energy of an additional helium atom to these clusters is evaluated when sitting in a first neighbouring octahedral site. This binding energy is

Table 2
Binding energies, E^B, for He atoms sitting in the Wigner–Seitz cells associated to the vacancy or the d-vacancies and E^B(He O) for He atoms sitting in the first neighbouring octahedral site (given in eV). The uncertainty of the estimates is one digit on the last decimal

Defect	E^B	E^B(He O)	Defect	E^B	E^B(He O)	Defect	E^B	E^B(He O)
He–V	+3.1	+0.4	He–V_{2a}	+3.1	+0.4	He–V_{2b}	+3.1	+0.3
He_2–V	+1.2	−0.3	He_2–V_{2a}	+2.9	+0.3	He_2–V_{2b}	+2.3	−0.6
He_3–V	+1.6	+0.5	He_3–V_{2a}	+1.9	−0.2	He_3–V_{2b}	+2.5	+0.5
He_4–V	+1.0	+0.0	He_4–V_{2a}	+1.6	−0.4	He_4–V_{2b}	+0.1	−1.8
He_5–V	+0.2	+0.3	He_5–V_{2a}	+1.5	+0.4	He_5–V_{2b}	+0.7	−0.6

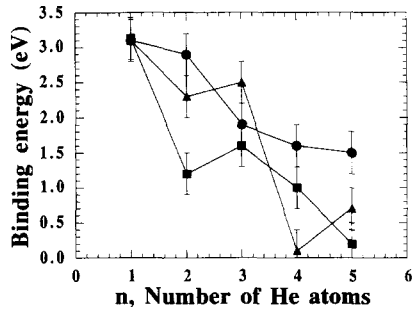

Fig. 3. Binding energy of a nth helium atom to a cluster already containing $n-1$ helium atoms as a function of n. Squares: the cluster contains one mono-vacancy; circles: it contains a di-vacancy of type a; triangles: it contains a di-vacancy of type b. Only equilibrium sites inside the associated Wigner–Seitz cells are considered.

found to be no systematic function of the filling of the Wigner–Seitz cell. It is remarkable for instance to notice that such a configuration may be unstable when the number of helium atoms in the Wigner–Seitz cell associated to a vacancy is as low as two, although it is stable when this number is five.

No second atom sharing a first neighbour octahedral site can be bound and the helium in second neighbour octahedral sites are found unbound as well. In other words, there exists a maximum number of helium atoms which can decorate a mono-vacancy or a di-vacancy. Since there are six equivalent octahedral sites first neighbouring a mono-vacancy and ten around a di-vacancy, with respect to Table 1, the maximum number of helium atoms which may decorate a mono-vacancy is eleven, it is fourteen around a di-vacancy of type a and twelve around a di-vacancy of type b.

Up to this point, only static configurations are considered. In what follows, the effect of temperature on clustering and cluster stability is considered. Clustering requires the defects to be mobile in order to interact. The kinetics involves thermal diffusion and the associated migration energies. Diffusion paths are shortly discussed in the next section.

3.2. Migration energies and mechanisms

Self interstitial diffusion by a mono-vacancy mechanism is known from experiment to be anisotropic [30,31]. The activation energies found are 1.71 eV and 1.63 eV for diffusion parallel and perpendicular to the c-axis, respectively. Since these activation energies represent the sum of the vacancy formation energy and the vacancy migration energy, this difference results from the difference in migration energies associated to diffusion jumps parallel to the c-axis or inside the basal plane. In the present model, the vacancy formation energy is 1.13 ± 0.01 eV. Migration energies were estimated according to the method described above and values of 2.0 ± 0.3 and 1.8 ± 0.3 eV are found parallel and perpendicular to the c-axis, respectively. The resulting activation energies, 3.1 ± 0.4 and 2.9 ± 0.4 eV, are substantially higher than the experimental values. The beryllium potential model used is responsible therefore. This one was designed on the basis of equilibrium properties of perfect beryllium single crystal. The results may however be consistent with a small anisotropy, although the differences between migration energies parallel to the a- and c-axes are beyond the uncertainties. The migration energies derived from the model for a and b types di-vacancies are 1.9 ± 0.4 and 1.7 ± 0.4 eV which are also consistent with a small anisotropy. The fact that the deduced activation energies (3.48 eV and 3.21 eV, respectively) are higher than those associated to the mono-vacancy mechanism is consistent with the experimental observation that the di-vacancy diffusion jump frequency is smaller than the mono-vacancy jump frequency. Since the migration energies are similar, this is the consequence of their lower concentration at thermal equilibrium (higher formation energy).

We now want to compare the migration energy of helium interstitials to that of mono-vacancies and, therefore, it is needed to identify the helium diffusion mechanism in a perfect beryllium matrix at constant temperature. This is done by molecular dynamics.

The beryllium simulation box is brought to thermal equilibrium at a temperature of 1100 K with one helium interstitial. This one is initially located at an octahedral site since this corresponds to the minimal configuration energy. Its trajectory is followed at thermal equilibrium over 50 ps. This is sufficient to observe more than 10 diffusion jumps. They all are found parallel to the c-axis. This computer experiment is repeated with starting the helium at a basal octahedral site and the same observation is made. Therefore, we conclude that the dominant interstitial helium diffusion mechanism in pure crystalline beryllium is parallel to the c-axis and it is observed to proceed by jump sequences between neighbouring octahedral sites parallel to the [0001] direction.

Interstitial helium thus appears to be quite mobile and its residence locations between diffusion jumps are identified. The saddle point is the basal octahedral location. Its migration energy is 0.6 ± 0.2 eV. This value is in very good agreement with the experimental estimates of 0.6 eV and 0.41 eV in [37,38], respectively. The interstitial helium migration energy is thus much smaller than the model vacancy migration energy. Simulations extending over 80 ps at high temperature ($T = 1273$ K) with a box containing vacancies did not allow to observe any diffusion jumps, which is consistent with the above mentioned difference.

In what precedes, the vacancy-helium cluster stability is discussed in terms of binding energies. By accounting for the high mobility of interstitial helium, this discussion may also be carried on in terms of a comparison between the migration energies of a helium atom *toward* a helium-

vacancy cluster and *from* a cluster. This comparison comes out in Fig. 4.

A first point is that the migration energy of a helium atom from an octahedral site toward a cluster is most generally much smaller than from a cluster to an octahedral site. In addition, within the accuracy of the present estimates, its value is independent of the number of already clustered helium and of whether if migrates to a vacancy or a vacancy cluster. Its value of 0.3 eV is even twice as small as the migration energy from one octahedral site to another within a perfect beryllium lattice. In contrast, migration energies from a cluster do depend on the number of helium atoms in this cluster. In the case of di-vacancies, however, no substantial difference is found between starting configurations with one or two clustered helium. This shows that the migration from one vacancy site is independent of whether the other is occupied or not.

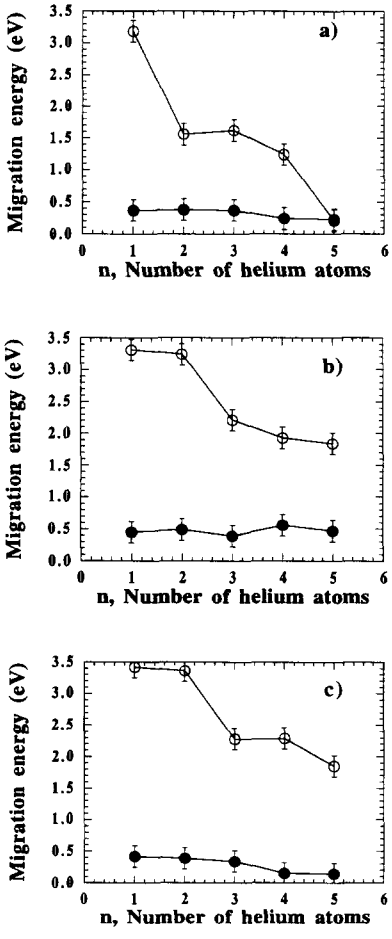

Fig. 4. Migration energies of a nth helium initially sitting in a first neighbouring octahedral site to a cluster already containing $n-1$ helium atoms (black circles) and from a cluster initially containing n atoms (open circles). (a) monovacancy, (b) V_{2a} di-vacancy, (c) V_{2b} di-vacancy.

3.3. Thermal effects

We now discuss the temperature dependence of the helium-vacancy cluster stability evidenced at 0 K. Two factors result from a change of temperature, which may affect the helium-vacancy cluster stability. These are the thermal expansion of the beryllium lattice and the change in the vibrational entropy which contributes to the free energy. No change in the role of the lattice anisotropy is to be expected since the c/a ratio is not found both experimentally and by simulation, to be significantly temperature dependent.

In what follows, the cluster stability is discussed on the basis of Helmholtz free energy difference estimates between a configuration with an independent helium interstitial and a He_{n-1}–V_m cluster on the one hand and a configuration with a He_n–V_m cluster. The estimates are performed as a function of temperature and the thermal lattice expansion is taken into account.

In the initial situation, one helium atom sits in an octahedral site first neighbour of a mono-vacancy or a di-vacancy, already decorated by a number of helium atoms.

The neighbouring helium is constrained at several (non-equilibrium) positions along a path to the vacancy. This path is arbitrarily chosen. For convenience, the constrained positions are selected in such a way that, after estimation of the mean thermodynamic force on the atom at these positions, they may serve as the node coordinates for the integration of this force along the path by means of a quadrature. This way, the thermodynamic work of the thermodynamic mean force may be obtained, which represents the free energy difference between the two configurations. The sign of this difference allows to conclude whether the He_n–V_m cluster is stable or not.

The free energy difference estimate is checked to be independent of the integration path and also of the method used to constrain the helium atom at a non equilibrium position. The calculation is repeated for all He_n–V_m configurations mentioned in Table 1 at temperatures of 0, 473, 873 and 1273 K, taking the thermal expansion of the beryllium lattice into account. The results are given in Fig. 5. The uncertainty in the estimate of the free energy differences is of the order of 0.2 eV.

It clearly comes out in Fig. 5 that, in all cases, the contribution of the vibrational entropy is smaller than the uncertainties. The same is found for the thermodynamic work required to constrain one helium atom from a second to a first neighbour octahedral site and from any site to a migration saddle point. The vibrational entropy thus only has a small effect on the cluster stability and Eqs. (15a) and (15b) provides, within the present model, reasonable estimates of binding energies at all temperatures up to 1273 K. Therefore, the results obtained by means of Eqs. (15a) and (15b) to situations where the helium bound to a mono-vacancy or a di-vacancy does not sit in the associ-

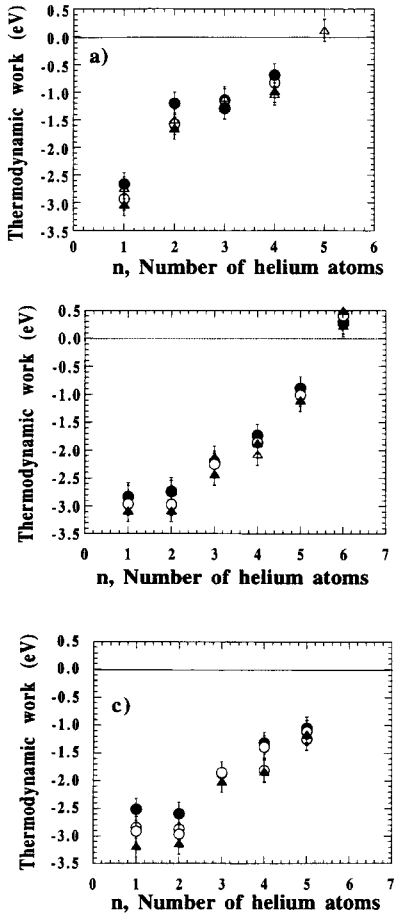

Fig. 5. Thermodynamic mean work required to constrain a nth helium from a first octahedral site to a helium-vacancy cluster already containing $n-1$ helium atoms. (a) The cluster contains one mono-vacancy; (b) it contains a di-vacancy of type a; (c) it contains a di-vacancy of type b. Results at 0 K are shown by open triangles, at 483 K by filled triangles, at 873 K by open circles and at 1273 K by filled circles.

ated Wigner Seitz cell, but in a neighbouring octahedral site can be considered as valid at non zero temperatures as well. The same is true for the estimates of migration energies.

4. Conclusion

The main result of this atomic scale study is that ten and more helium atoms may be trapped at a single vacancy or at a di-vacancy. This number is not significantly temperature dependent and 0 K estimates are thus reasonable. The fact that beryllium vacancy diffusion obeys an Arrhenius law fairly well indicates that the relative population of di-vacancies is small and of tri- and large vacancy groups negligible. This is the reason why they are not considered in the present study, also the study of helium trapping by larger vacancy clusters is no problem.

The binding energy of helium atoms to point defect traps is, however, much dependent on the number of helium atoms per trap and this should influence the statistics of helium-vacancy cluster populations. Another parameter which affects this population is the migration energy. The estimated beryllium vacancy migration energy is larger than the experimental value, suggesting that the model potential could be improved in this respect. The helium migration energy resulting from the mean field approximation and the embedded atom model may be better reasonable and its estimate *from* and *to* a helium-vacancy cluster may be useful for a kinetic study.

Unfortunately, such small clusters are hardly characterised experimentally, which should be necessary for a better assessment of the model. Computer performances available at present, together with the evidence shown above that vibrational entropy only has a limited influence on the cluster stability makes a similar study for extended defects realistic. Work is in progress in this direction.

References

[1] W.G. Wolfer, T.J. Mc.Carville, Fus. Tech. 8 (1985) 1157.
[2] L. Sannen, F. Moons, Y. Yao, CEN/SCK Report FT/Mol/93/07, 1993.
[3] J.M. Beeston, L.G. Miller, E.L. Wood, R.W. Moir, J. Nucl. Mater. 122&123 (1984) 802.
[4] R.S. Barnes, J. Nucl. Mater. 11 (1964) 135.
[5] M.C. Billone, C.C. Lin, D.L. Baldwin, Fus. Tech. 19 (1991) 1707.
[6] C. Nardi, ENEA Report RT/NUCL/91/24, 1993.
[7] F. Scaffidi-Argentina, FZKA-5632, 1995.
[8] G.A. Sernyaev, Vopr. Atom. Nauk. Tekhn. 2 56 (1991) 16.
[9] D. Harries, M. Dalle-Donne, FZKA-5778, 1996.
[10] F. Moons, CEN/SCK Report FT/Mol/95/03, 24-29, 1995.
[11] S. Nosé, J. Chem. Phys. 81 (1984) 511.
[12] S. Nosé, Progr. Theor. Phys. Suppl. 103 (1991) 1.
[13] A. Nordsieck, Math. Comput. 16 (1962) 22.
[14] L. Verlet, Phys. Rev. 159 (1967) 98.
[15] G.S. Grest, B. Dünweg, K. Kremer, Comp. Phys. Comm. 55 (1989) 269.
[16] M. Born, Th. von Karman, Phys. Z. 13 (1912) 297.
[17] M.W. Finnis, J.E. Sinclair, Philos. Mag. A50 (1984) 45.
[18] M. Igarashi, M. Khantha, V. Vitek, Philos. Mag. B63 (1991) 603.
[19] G.J. Ackland, G. Ticky, V. Vitek, M.W. Finnis, Philos. Mag. A56 (1987) 735.
[20] J.K. Nørskov, N.D. Lang, Phys. Rev. B21 (1980) 2131.
[21] M.J. Stott, E. Zaremba, Phys. Rev. B22 (1980) 1564.
[22] K.W. Jacobsen, J.K. Nørskov, M.J. Puska, Phys. Rev. B35 (1987) 7423.
[23] M.J. Puska, R.M. Nieminen, M. Manninen, Phys. Rev. B24 (1981) 3037.
[24] M. Mannimen, J.K. Nørskov, M.J. Puska, C. Umrigar, Phys. Rev. B29 (1984) 2314.

[25] N.D. Lang, J.K. Nørskov, Phys. Rev. B27 (1983) 4612.
[26] N. Esbjerg, J.K. Nørskov, Phys. Rev. Lett. 45 (1980) 807.
[27] M.J. Puska, R.M. Nieminen, Phys. Rev. B43 (1971) 12221.
[28] A.A. Abrahamson, Phys. Rev. 178 (1969) 76.
[29] V.I. Gaydaenkoand, V.K. Nikulun, Chem. Phys. Lett. 7 (1970) 360.
[30] J.M. Dupouy, J. Mathie, Y. Adda, Mem. Sci. Rev. Met. 63 (1966) 4811.
[31] M. Beyeler, D. Lazarus, Mem. Sci. Rev. Met. 67 (1970) 395.
[32] C.H. Bennet, in: Diffusion in Solids: Recent Developments, eds. A.S. Norwock and J.J. Burton (Academic Press, New York, 1975) p. 75.
[33] M. Hou, A. Hairie, B. Lebouvier, E. Paumier, N. Ralantosson, O. Hardouin Duparc, A.P. Sutton, Mater. Sci. Forum 207–209 (1996) 249.
[34] A.P. Sutton, in: Atomic Simulation of Materials, eds. V. Vitek and D.J. Srolowitz (Plenum, New York, 1988) p. 268.
[35] W.D. Wilson, C.L. Bisson, M.I. Baskes, Phys. Rev. B24 (1981) 5616.
[36] J.R. Beeler Jr., in: Series Defects in Crystalline Solids, eds. S. Amelinckx, R. Gevers and J. Nihoul (North-Holland, Amsterdam, 1983).
[37] P. Jung, J. Nucl. Mater. 202 (1993) 210.
[38] A.G. Bespalov, Tr. Fiz.-Energ. Inst. (1974) 443.